IET Renewable Power Generation

Research Article

IET Journals
The Institution of Engineering and Technology

Quantifying benefits of wind power diversity in New Zealand

ISSN 1752-1416
Received on 12th September 2018
Revised 28th January 2019
Accepted on 22nd February 2019
doi: 10.1049/iet-rpg.2018.5410
www.ietdl.org

Dougal McQueen[1], Alan Wood[2] ✉

[1]*Electric Power Engineering Centre, University of Canterbury, Christchurch, New Zealand*
[2]*Electrical and Computer Engineering, University of Canterbury, Christchurch, New Zealand*
✉ *E-mail: dougal.mcqueen@epecentre.co.nz*

Abstract: Wind integration studies often focus on the capacity value of wind power without considering Unit Commitment and Economic Dispatch or resolving requirements for ancillary services. Here, a novel method for simulating wind power time series with sufficient temporal span to support capacity studies and temporal resolution to support UCED studies is developed. Wind speed time series (WSTS), with 6 h temporal and 0.7 × 0.7 degree spatial resolutions, are extracted from the ECMWF-interim reanalysis, interpolated, scaled, and imputed so that they are representative of a point wind speed measurement with a 5 min temporal resolution. Imputation is made using a wavelet multi-resolution analysis approach that ensures temporally consistent correlations while accounting for heteroskedasticity. WSTS are transformed to power using wind power plant power curves, low-pass filters, and a Markov Chain model of operational efficiencies. The wind power model is validated using a set of measurements made at wind power plants (WPPs) in New Zealand and used to simulate power time series for 2 GW portfolios of WPPs representing compact, disperse, diverse, and business-as-usual portfolios. Metrics for dependability, variability, and predictability are applied to quantify the benefits of spatial diversification.

1 Introduction

Wind power is one of the least cost methods for electricity generation and along with its scaleability and lack of emissions, this has led to large numbers of wind power plants (WPP) being integrated into power systems. However, the intermittency of wind and the largely passive reaction of wind turbines (WT) leads to certain levels of variability and unpredictability in wind power output. Further, WTs commonly use asynchronous generators and increasing the penetration of wind power leads to the relative reduction in power system inertia. Hence, increasing the installed capacity of wind power can require additional reserves and interruptible loads, referred to as secondary control mechanisms [1], to balance the power system. As power plants capable of supplying reserves can have large capital costs and lead times for building plant are long, it is requisite that integration studies are undertaken to quantify the necessary reserves for envisaged wind power development scenarios. Integration studies that focus on reserves requirements are classified as unit commitment and economic dispatch studies [2]. The intermittent and stochastic nature of wind power makes balancing the power system in transmission and distribution networks complex; requiring procurement of reserves, scheduling and control of assets, and applying new forecasting methods as they are developed [3].

Studies such as that presented by Sturt and Strbac for estimating the aggregate wind power output for the UK in 2030 have a temporal resolution of 1 h [4]. However, a requirement of the wind power time series simulated here is that they can be used to support system stability studies, given the integration of different portfolios of WPPs. This requires a temporal resolution of 5 min requiring a novel time-series model. Further, this study also seeks to evaluate the differences in power output from a portfolio of a few large WPPs compared with that from many small WPPs. Studies such as Sturt and Strbac's [4] simulate sets of time series that are regionally representative and do not simulate the power output from individual WPPs, hence this novel method using wavelet decomposition has been developed.

The wind generation investigation project (WGIP) was undertaken in New Zealand (NZ) by the system operator to address concerns over large ramp rates observed in the Manawatu during 2004 [5, 6]. The WGIP, conducted in 2007, was accompanied by other integration studies by various stake holders [7–9]. The number of integration studies conducted worldwide lead to the IEA producing guidelines to assist system operators with managing wind power integration [2]. Many integration studies conclude that one way of reducing stress on the power system is through spatial diversification [10, 11]. However, most studies fall short of quantifying that benefit.

Secondary control of the NZ power system is primarily achieved by the NZ electricity market (NZEM). The NZEM uses 30 min windows, each window constituting a trading period, with gate closure 2 h prior to the trading period (at the time of this study). As changes in demand and generation are faster than the reaction of the NZEM, a reserves market with a window of 5 min is also operated. These temporal spans provide the basis for metrics of variability (changes in power output or ramps over 5 min) and predictability (the error in power forecasts with a 2 h horizon using a 30 min window). For this study, power forecasts are made assuming persistence, as standard wind forecasting methods provide little additional benefit for horizons of <6 h [12]. Recent developments in wind power forecasting have greatly improved results but these are often site-specific and tailored to specific applications [13], whereas a generic method is required. A dependability metric is also used, describing how much power can be relied upon at any time and is measured using the standard deviation of power.

To quantify the benefits of spatial diversification sets of wind power, time series are required. The sets of time series must replicate the variability of the WPPs, the spatio-temporal correlations between WPPs, and be congruent with other forms of generation and demand so that the impact on the power system can be evaluated.

2 Scenarios

To demonstrate the potential benefits from spatial diversification, of WPPs in NZ, scenarios for wind power development have been constructed. The location of the WPPs in the scenarios is taken from media releases that cover either commissioning, consenting, or proposal. Four scenarios have been developed, each comprising 2 GW capacity. A compact scenario comprises seven WPPs, nominally 300 MW, located in the lower North Island, a disperse

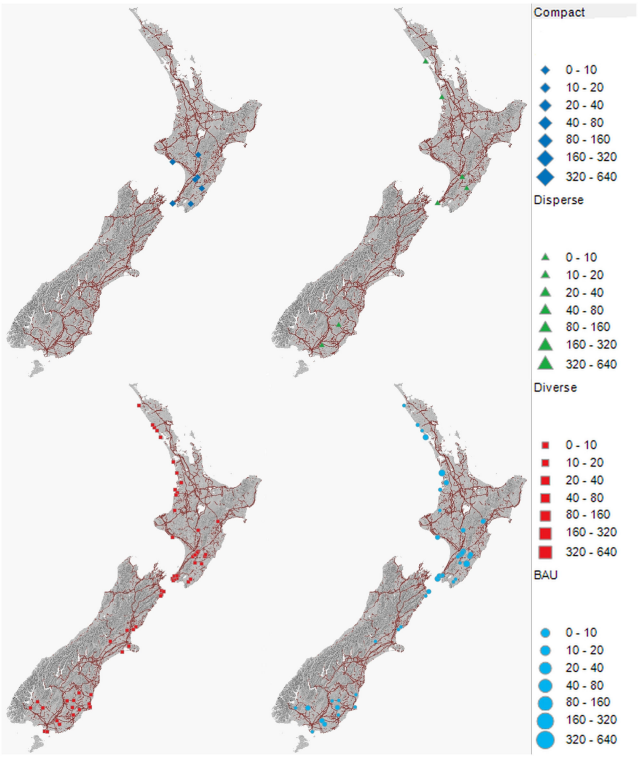

Fig. 1 *Scenarios each comprising 2 GW capacities. Top left: compact, top right: disperse, bottom left: diverse, bottom right: business as usual (BAU)*

scenario comprises seven WPPs spread throughout NZ, and a diverse scenario comprises 70 WPPs (nominally 30 MW) spread throughout NZ. A business-as-usual scenario comprises the set of WPPs presently operational, plus WPPs with capacities consistent with those operational, to make up the 2 GW portfolio. The scenarios are presented in Fig. 1. It is assumed that the WPPs comprise approximate square arrays of Vestas V80 2.0 MW WTs [14], with capacity factors of 40%.

3 Wind speed simulation

Coherent sets of wind power time series are obtained by simulating wind speed time series (WSTS) for each WPP and transforming these to power. The WSTS must be representative of the wind incident on the WPPs individually and have correlations that are temporally and spatially consistent. Coarse resolution WSTS are extracted from the ECMWF ERA-interim Numerical Weather Prediction (NWP) model, which is freely available and provides wind speeds representative of a 10 m height, on a grid with reasonable spatial (0.7 × 0.7 degree) and temporal resolutions (6 h) [15]. The WSTS requires interpolation to WPP locations, scaling to be representative of the wind incident on the WPP, and imputation to obtain the desired temporal resolution. Many integration studies increase temporal and spatial resolutions, or downscale, using meso-scale models [11]; however, here numerical methods are used that require fewer resources.

There are many numerical methods for interpolation of WSTS such as Kriging [16]; however, it is found that the differences between various methods are relatively small [17]. Here, the WSTS are interpolated using two-dimensional cubic splines, and scaled by a ratio so that the resultant power time series have capacity factors equal to 40%. The scaling of a WSTS is shown in (1). A set of wind speed measurements made at 21 meteorological masts, located throughout NZ and erected for wind prospecting purposes, are used to validate the interpolation function as detailed by McQueen [17]. The dataset is similar to that used in the wind generation integration project [3].

$$u_N(t) = S_{(\theta,N)} \times u_M(t) \tag{1}$$

where u is the 10 min mean wind speed, N is the turbine index, t is time, θ is the wind direction sector, S is the speed up, and M denotes the meteorological mast.

The imputation of the WSTS increases the temporal resolution from 6 h to 5 min. A model that is spatially and temporally congruent is developed which in effect characterises turbulence. The model applies wavelet multi-resolution analysis (WMA) and is validated using the set of wind speed measurements [18].

A wavelet is a finitely bounded function that is square integrable as presented in (2). This means that the wavelet is a short sequence with an oscillatory shape, with some wavelets being similar to a discretised damped sine wave. A wavelet transform decomposes a time series, by deconvolving the time series by the wavelet, resulting in a residual time series and a wavelet series. The residual time series and wavelet series have temporal resolutions half that of the starting time series. Wavelets are numerically particular so that the space defined by the scale and translating the wavelet series is orthogonal to the residual time series. The scale can be considered as the wavelet space equivalent of frequency, and the translation the wavelet space equivalent of time.

$$\left\{\psi_{j,\tau}(t) = \frac{1}{\sqrt{2^j}}\psi\left(\frac{t-2^j\tau}{2^j}\right)\right\}_{(j,\tau)inZ^2} \tag{2}$$

where ψ is the mother wavelet, j is the scale, τ is the translation, and Z is the set of integers.

$$\langle u(\tau, 2^j), \Psi(j,\tau)\rangle = \int_{-\infty}^{\infty} u(t)\frac{1}{\sqrt{j}}\psi^*\left(\frac{t-\tau}{j}\right)\mathrm{d}t \tag{3}$$

where Ψ is the wavelet coefficient series, t is time, and * denotes the complex conjugate.

The wavelet transform is applied recursively to a wind speed time -series, by dilating the wavelet, so that a set of wavelet series and a residual time series, with a coarse temporal resolution, is obtained. The set of wavelet series has scales that are spread dyadically, i.e. having central scales that are spread as powers of two as expressed in (3). Here, the wavelet decomposition is structured so that the temporal resolution of the residual time series is 6 h to marry with the ECMWF-interim model resolution. Hence, the wavelet series have scales of 6, 3, 1.5, 0.75, and 0.375 h.

The wavelet decomposition of the total wind speed data set results in a data structure with three dimensions: scale, translation, and the distance between time series. This structure is identified using measures of cross-correlation (4), auto-correlation (5), and correlation (6); respective of scale, translation, distance. Simulation of a three-dimensional data-structure is complicated; however, the dimensionality of the dataset is effectively reduced by minimising the cross-correlation by careful selection of the wavelet. Of all the wavelets in the Wavelet toolbox for Matlab [14], the Beylkin wavelet results in the lowest cross-correlation, sufficiently small to allow wavelet series of adjacent scales to be considered independent.

$$R(\Psi_n(j), \Psi_n(j+1)) = \sum_{\delta=[-(1/4),(1/4)]}\sum_{\tau=1}^{T}\{(\Psi_n(j,\tau) - \overline{\Psi_n(j,\tau)} \times (\Psi_n(j+1,\tau+\delta) - \overline{\Psi_n(j+1,\tau+\delta)}) \tag{4}$$

$$R(\Psi_n(j,\tau), \Psi_n(j,\tau+\delta)) = \sum_{\tau=1}^{T}\{(\Psi_n(j,\tau) - \overline{\Psi_n(j,\tau)}) \times (\Psi_n(j,\tau+\delta) - \overline{\Psi_n(j,\tau+\delta)})\} \tag{5}$$

where R is the Pearson's correlation coefficient, n is a measurement, and $\Psi_n(j,\tau)$ is the temporal average of the wavelet coefficients.

$$R(\Psi_n(j),\Psi_m(j)) = \sum_{\tau=1}^{T}\{(\Psi_n(j,\tau)-\overline{\Psi_n(j,\tau)}) \times (\Psi_m(j,\tau)-\overline{\Psi_m(j,\tau)})\} \quad (6)$$

where m is a second measurement.

Using the decomposition of the measured WSTS, it is found that the relationship between the mean square, or power, of the wavelet series and the scale is well approximated by a log-log linear function, similar to Kolmogorov's law [19]. The assumption of a log-log linear function allows the WMA model to be extrapolated [17]. The WMA model is extrapolated to scales of 11.25 and 5.26 min, so that the simulated time series have a temporal resolution of 1.81 min; greater that the 5 min criteria for determining ramp rates. It is found that the correlation at any scale is well approximated by a log-linear function of the separation distance between wind speed measurement locations, as shown in Fig. 2. As the minimum separation distances in the WGIP dataset are >1 km and the dataset does not resolve scales of 11.25 and 5.26 min, additional data from the Mt Stuart wind farm are used to inform the log-linear correlation functions. The distance relationship is a wavelet domain equivalent to Davenport's model of coherence.

The decomposition of the time series into a set of wavelet series allows a relationship between the wavelet series and the residual time series to be established. It is found that the magnitude of the wavelet series is related to the magnitude of the residual time series, and this is modelled using a Taylor's transform as shown in (7). The application of the Taylor's transform accounts for gustiness, which is literally interpreted in the statement 'it is gusty when it is windy'. If the Taylor's transform is not applied, then the simulated WSTS will be homoskedastic, and the resulting power time series will not have temporally correct ramp rates.

$$\Psi_n^{(T)}(j,\tau) = \frac{\Psi(j,\tau)}{\bar{u}(t)^a} \quad (7)$$

where a is the Taylor exponent, and T represents the Taylor transformed variable, and $\bar{u}(t)$ is the wind speed at time t averaged over a time window of 360 min.

$$\Psi n^{(TJ)}(j,\tau) = \gamma + \eta \sinh^{-1}\left(\frac{\Psi_n^{(T)}(j,\tau)-\varepsilon}{\lambda}\right) \quad (8)$$

where J represents the Johnson transformed variable, γ and η are shape parameters, ϵ is the location parameter, and λ is the scale parameter.

Sets of the WSTS are simulated by constructing a wavelet structure for each WPP. The residual time series in the wavelet structure is filled using values from the interpolated and scaled ECMWF-interim WSTS. Each wavelet series in the wavelet structure is filled with a sequence of random numbers that have auto-correlations and correlations enforced using a correlated innovation matrix (CIM) method as shown in (9). The Box-Jenkins method using correlograms and partial-correlograms identifies the $\Psi_n^{(TJ)}(j)$ series as an over-differenced AR processes with a model order of 1 [20]. The CIM method works by multiplying the innovation matrix in the AR process by the Cholesky decomposition of the correlation matrix calculated using the log-linear distance relationship.

$$\begin{aligned}\Psi_n^{(TJ)}(j,\tau) = {} & A_\alpha(j)\times\Psi_n^{(TJ)}(j,\tau-\alpha) \\ & + A_{\alpha-1}(j)\times\Psi_n^{(TJ)}(j,\tau-(\alpha-1)) \\ & + \cdots + A_1(j)\times\Psi_n^{(TJ)}(j,\tau-1) + \zeta\times e_t\end{aligned} \quad (9)$$

where A_α is the AR coefficient of order α, ζ is the CIM weighting matrix, and e is the innovation matix.

The shape of the probability distributions for the measured wavelet series are non-Gaussian. As simulations are initiated from normally distributed random numbers, a Johnson transform, as shown in (8), is applied to modify the simulated wavelet-series so that the shape of their probability distributions approximates that of the measured [17]. Inverse wavelet transformations are then applied to obtain a WSTS for each WPP.

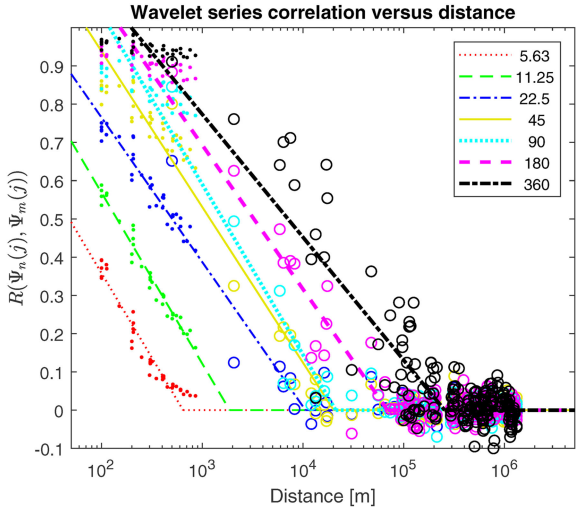

Fig. 2 *Correlation as a function of separation distance for wavelet series with scales from 5.63 min through 360 min. Points represented using circles derive from the wind speed data set, points represented using dots derive from the Mt Stuart data. Lines present best fit log-linear regressions*

4 Wind speed to power transform

WSTS are transformed to power by accounting for the effective steady state and dynamic characteristics of the WPP separately. The steady-state transform, which can be reconciled as modification to the bulk wind flow from the topography, is modelled using a generic WPP power curve. The generic WPP power curve is obtained by applying a Gaussian distribution of speed-ups to the WT power curve as shown in (10). A speed-up standard deviation of 0.065 is obtained from measurements made at the Mt Stuart Wind Farm with the mean speed-up equalling one.

$$P_S(u) = \int_{q=0}^{1} P(u\times S_{\mu_g,\sigma_g}(q))\,\mathrm{d}q \quad (10)$$

where P is power, S is a speed-up, d is wind direction sector, and q is probability.

The dynamic transform, which can be reconciled as characterising the inertial and spatial integration of the WPP, is modelled using a simple low-pass filter (LPF) as shown in (11). The LPF multiplier (M_c) and exponents (M_e) depend on the size of the WPP, and are calculated through simulation of power time series for WPPs comprising square arrays of Vestas V80 2.0 MW turbines. The WMA model, as described in [17], is used to simulate the WSTS incident on each WT. These WT WSTS are converted to power using the WT power curve and aggregated to find a WPP power time series. A power time series is simultaneously derived using a WPP power curve applied to a single turbine WSTS that has been low-pass filtered. The LPF multiplier and exponents are found by minimising root-mean-square difference in the power spectral densities (PSD) between the two power time series, resulting in a LPF multiplier of 151 s and an exponent of 0.57 [17].

$$u_{\omega'} = F'\left\{F(u)\frac{1}{1+M_c\times N^{M_e}\times\omega}\right\} \quad (11)$$

where ω is frequency, F denotes a Fourier transform, F' the inverse Fourier transform, N the number of turbines, M_c the time constant, and M_e the LPF exponent.

The simulated power from the WPP (P) is the sum of the power supplied by all of the WTs given unrestricted operation. In reality, a

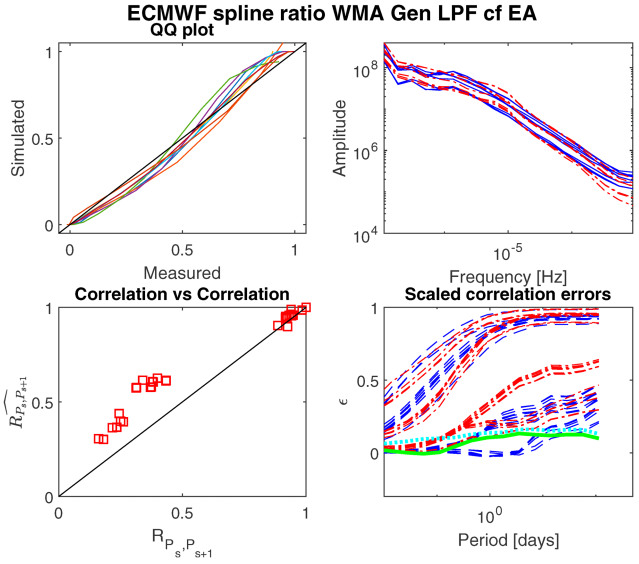

Fig. 3 *Wind power validation*

WPP incurs losses due to electrical efficiency and WPP operation. Electrical losses are relatively small and vary with the power, and are accounted for in WPP power curve. The operational losses occur due to faults and maintenance of the WPP, and can result in large instantaneous changes in output. A Markov Chain (MC) model for the operational efficiency is constructed using measurements made at a set of eight WPPs, similar to the model described by Sulaeman [21]. A full explanation of the MC model is available in [17, 22]. Time series of the operational efficiency are obtained for each WPP and percentile values calculated. Transition matrices are formed from these and the average of the transition matrices used to define a generic MC model. The mean operational efficiency from measurements is 95% and this is replicated by the MC model [17].

5 Validation

Measured power time series, from a set of eight WPPs in NZ, are used validate the wind power model. The measurements have a temporal resolution of 5 min and a duration of 7 months. Power time series are simulated for the period that is coincident with the measured power time series. In summary, WSTS are derived from the ECMWF-interim NWP model, interpolated, scaled, and imputed. The WSTS are smoothed using a LPF, transformed to power using generic WPP power curves, and modified to account for the operation efficiency using the MC model. The WSTS are scaled such that the total energy of a simulated time series equals that of the equivalent measured.

The wind power time series are compared with the measured time-series in Fig. 3. The top left graph presents a Quantile-Quantile (QQ) plot, each line representing a WPP, which shows good agreement between the probability distribution functions of the simulated and measured time series. The top right graph presents a periodogram with PSDs derived from measured values shown as blue lines and from simulations as dash dotted red lines. The simulated PSDs tend to underestimate variability for frequencies above 10^{-4} Hz, reflecting the assumption that WPPs comprise square arrays which results in WPPs with less spatial extents than their real-world counterparts. The bottom left graph presents simulated versus measured correlations as shown in (12). It is seen that the model generally over predicts the correlation between power time series, i.e. real-world WPPs behave with greater independence than the simulations suggest.

$$R_{P_r,P_s} = \frac{\sigma_{P_r,P_s}}{\sigma_{P_r} \times \sigma_{P_s}} \tag{12}$$

where R is the Pearson's correlation coefficient, r and s are different WPPs, σ_{P_r} is the variance of power from WPP r, and σ_{P_r,P_s} is the covariance between the time series.

A measure of the correlation as a function of the temporal span is the scaled correlation. For a particular scale, power time series pairs are broken into segments of the corresponding length (as presented in (13)), the correlation coefficient for each pair of segments is derived, and the average of these correlation coefficients is calculated as presented in (14). The lower right graph presents scaled correlations. The dashed blue lines represent the scaled correlations between pairs of power time -series from measurements and the dash dotted red lines result from simulations. The scaled correlations show that at low scales, the correlation between WPPs is small and increases as the scale becomes larger. An indication of the difference between the sets of simulated and measured scaled correlations is given by the mean bias (shown by the solid green line), and the root mean squared (shown using the dotted cyan line). For scaled correlations with periods of <6 h, simulated data derive from the WMA model and those with periods longer than 6 h derive from the NWP model. This shows the WMA model accurately models the scaled correlations while there are greater errors introduced from the NWP model.

$$K(j) = floor\left(\frac{T}{j}\right) \tag{13}$$

where K are the power time-series segment, T is the total time, and j is the scale.

$$\bar{R}_{P_r,P_s}(j) = \frac{1}{K}\sum_{k=1}^{K} R_{P_r(k),P_s(k)} \tag{14}$$

where $\bar{R}_{P_r,P_s}(j)$ is the scaled correlation between power time series from WPPs r and s at a scale of j.

6 Results

The wind power model is used to simulate power time series for each of the envisaged WPPs in the scenarios for the year of 1998. The results presented in Fig. 4, where the top left graph presents a short extract during which Cyclone Bola crossed NZ. This storm caused significant damage, and it is of interest to see how it might have impacted the power of the various scenarios. It is seen that the power from a compact scenario has a much greater changes in power than the disperse or BAU scenarios. The diverse scenario provides the smoothest power output. The top right graph presents probability density functions for the power over the entire year of 1998. It is seen that a compact scenario has a more extreme shape to its probability distribution, with greater chance of near zero and near maximum outputs than the other scenarios. The differences in the shapes of the PDFs is reflected in the standard deviation for the scenarios presented in Table 1 where it is seen that a compact scenario has a standard deviation 28% greater than the diverse scenario. This means that a compact scenario of WPPs will produce power with lower dependability than a disperse or diverse scenarios.

The lower left graph presents ramp rates and it is seen that the compact and disperse scenarios have near identical variability, whereas the diverse scenario results in ramp rates 25% of the compact scenario. The distribution of ramp rates has a slight positive bias; the magnitude of ramp rate increases with a probability of occurrence equating to once per week is 10% greater (for disperse and BAU scenarios) than the equivalent ramp down.

The lower right graph presents forecast errors for the scenarios; the forecast errors for the compact scenario are 45% greater than for the other scenarios. It is seen that the distribution of forecast errors is skewed in favour of negative errors, once per week forecast errors having ~20% greater magnitude of under-prediction than the equivalent over prediction.

The BAU case exhibits a balance between the diverse and compact scenarios with a variance 83% of the compact scenario

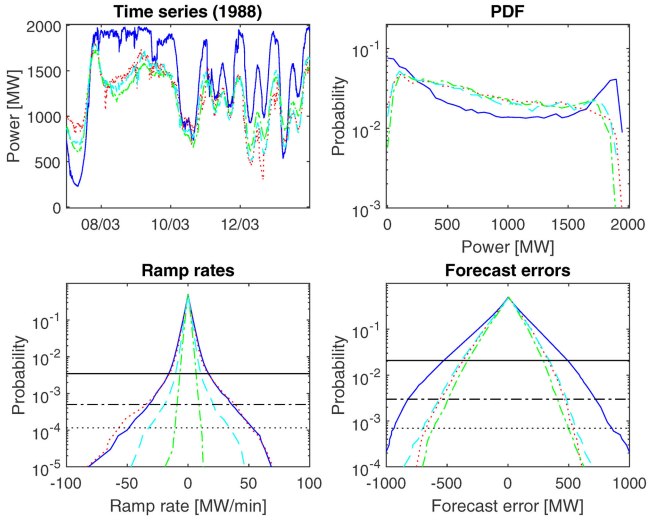

Fig. 4 *Power simulation results for scenarios: solid blue (compact), dash dot green (disperse), dotted red (diverse), dashed cyan (BAU). Horizontal solid black lines correspond to events with a probability of occurrence of once per day, dash-dotted with events that occur once per week, and dotted with events that occur once per month*

Table 1 Results from wind power simulations for scenarios. Ramp rates and forecast errors are representative of events with a probability of occurrence of once per week

Scenario	Compact	Disperse	Diverse	BAU
mean, MW	799	799	799	799
standard deviation, MW	664	534	519	551
+ve ramp rate, MW	−33	−32	−8	−18
−ve ramp rate, MW	35	37	8	20
+ve forecast error, MW	−758	−514	−487	−563
−ve forecast error, MW	636	438	397	457

but 6% higher than the diverse scenario, ramp rates are half those for the compact scenario but twice the diverse scenario, and forecast errors are 75% of the compact scenario and 15% greater than the diverse scenario.

7 Conclusion

The integration of WPPs into electricity networks can lead to the need for increased reserves so that power quality is managed. Many integration studies conclude that the impact of wind power on the power system can be reduced through spatial diversification. However, few of these studies provide methods for comprehensively quantifying the impact of specific wind power portfolios.

This paper has outlined a method that simulates power time series with the correct spatial and temporal correlations. The method uses WSTS from the ECMWF-interim Numerical Weather Prediction model. The WSTS are interpolated, scaled, and imputed so that they are representative of the wind speed incident on WPPs. The imputation uses a wavelet-multi-resolution analysis approach ensuring temporally and spatially consistent correlation. The WSTS are transformed to power using a LPL applied to the WSTS, a generic WPP power curve, and a MC model to capture operational efficiency.

Power time series are simulated and compared with a set of measured power time series from WPPs located in NZ, showing the model has good accuracy. The model is applied to simulate 2 GW portfolios of wind power scenarios in NZ. It is shown that a compact portfolio will result in lower dependability, a disperse portfolio will have greater predictability, and a diverse portfolio will have lower variability. The business-as-usual scenario indicates the development of wind power in NZ to date has achieved some of the benefits of spatial diversification, however greater benefits could be accrued through coordinated.

8 Acknowledgments

This work presents the results of the PhD thesis of Dougal McQueen completed as part of the GREEN Grid project funded by Ministry of Business Innovation and Employment (CONT-29328-EMRTR-UOC), Transpower, and the Electricity Engineers' Association.

9 References

[1] Ackermann, T: '*Wind power in power systems*' (Wiley, UK, 2005, 1st edn.)
[2] IEA: '*Expert group report on recommended practices; 16. Wind integration studies*' (IEA, Finland, 2016)
[3] Yong, L., Wen, Z., Cao, Y., *et al.*: 'A combined forecasting approach with model self-adjustment for renewable generations and energy loads in smart community', *Energy*, 2017, **129**, pp. 216–227
[4] Sturt, A., Strbac, G.: 'Times-series modelling for the aggregate Great Britain wind output circa 2030', *IET Renew. Power Gener.*, 2013, **1**, pp. 36–44
[5] McQueen, D., Wong Too, P., White, G.: 'Wind power variability and forecast accuracy in New Zealand', Garrad Hassan Pacific Pty, 2007. Available at http://www.ea.govt.nz/our-work/programmes/pso-cq/wgip/
[6] Transpower: 'Effect of unpredictability of wind generation output on pre-dispatch processes, Investigation 1- Part A', Electricity Authority, 2007
[7] Rasmussen, I.M.: 'Wind power integration in New Zealand: a scenario analysis of 15–25% wind power in the electricity market in 2025'. Masters thesis, Technical University of Denmark, 2008
[8] Strbac, G., Pudjianto, D., Shakoor, A., *et al.*: 'The system impacts and costs of integrating wind power in New Zealand', Electric Power Optimization Centre, 2008. Available at http://www.epoc.org.nz/workshops/ww2008/NZWindIntegrationCostsPhase-IIReportFinal.pdf
[9] Energy Link, MWH NZ: '*Wind energy integration in New Zealand*' (Ministry of Economic Development Energy Efficiency and Conservation Authority, New Zealand, 2005)
[10] Dowds, J., Hines, P., Ryan, T., *et al.*: 'A review of large-scale wind integration studies', *Renew. Sust. Energy Rev.*, 2015, **49**, pp. 768–794
[11] Manobianco, J., Alonge, C., Frank, J.: 'Development of regional wind resource and wind plant output datasets for the Hawaiian islands', National Renewable Energy Laboratories, 2010
[12] Metservice: '*Response to consultation paper: wind forecasting and integration options*' (Electricity Authority, New Zealand, 2010)
[13] Feng, C., Sun, M., Cui, M., *et al.*: 'Characterizing forecastability of wind sites in the United States', *Renew. Energy*, 2018, **133**, pp. 1352–1365
[14] Vestas: '*General specification, V80-2.0 MW 50 Hz VCS*' (Vestas, Denmark, 2010)
[15] Dee, D.: 'The ERA-interim reanalysis: configuration and performance of the data assimilation system', *Q. J. R. Meteorol. Soc.*, 2011, **137**, (656), pp. 553–597
[16] Luo, W., Taylor, M., Parker, S., *et al.*: 'A comparison of spatial interpolation methods to estimate continuous wind speed surfaces using irregularly distributed data from England and Wales', *Int. J. Climatol.*, 2008, **28**, pp. 947–959
[17] McQueen, D.: 'Quantifying the benefits from the spatial diversification of wind power in New Zealand'. PhD thesis, University of Canterbury, 2017
[18] Mallat, S.: '*A wavelet tour of signal processing*' (Academic Press, USA, 2008, 3rd edn.)
[19] Stull, R.B.: '*An introduction to boundary layer meteorology*' (Kluwer Academic, The Netherlands, 2003)
[20] Lütkepohl, H.: '*New introduction to multiple time series analysis*' (Springer, Germany, 2007)
[21] Sulaeman, S., Benidris, M., Mitra, J.: 'A method to model the output power of wind farms in composite system reliability assessment'. North American Power Symp. (NAPS), Pullman, USA, 2014
[22] McQueen, D., Wood, A., Miller, A.: 'Dynamic wind power simulation'. 14th Wind Integration Workshop, Brussles, Belgium, 2015